IEEE Access
Multidisciplinary | Rapid Review | Open Access Journal

Received 17 July 2023, accepted 31 July 2023, date of publication 7 August 2023, date of current version 10 August 2023.

Digital Object Identifier 10.1109/ACCESS.2023.3302347

RESEARCH ARTICLE

Wireless Power Transmission System for Vehicle Based on Multi-Transmitter Coils Array

QI LE[1,2], RUIMING WU[1,2], JIANGYU CHEN[1,2], MEILING HUANG[1,2], YANG FU[1,2], FENG HUANG[1,2], LIJUN WANG[3], SHAN DU[4], AND QIPENG LI[1,2]

[1]School of Mechanical and Energy Engineering, Zhejiang University of Science and Technology, Hangzhou, Zhejiang 310023, China
[2]Zhejiang Provincial Key Laboratory of Food Logistics Equipment and Technology, Hangzhou 310023, China
[3]School of Automation and Electrical Engineering, Zhejiang University of Science and Technology, Hangzhou, Zhejiang 310023, China
[4]Zhejiang Linix Motor Company Ltd., Jinhua, Zhejiang 321000, China

Corresponding author: Yang Fu (yangfu@zust.edu.cn)

This work was supported in part by the National Natural Science Foundation of China under Grant 51905486, and in part by the Basic Research Program of Zhejiang Province under Grant LGG20F020008.

ABSTRACT Wireless power transmission technology based on coil coupling has been widely applied in various fields. However, the performance of the system is affected by the malposition of the transmission coil-couple, which is inevitable in the wireless power transmission system (WPTS). In this study, a multi-transmitter coil array is proposed to build a more uniform magnetic flux density for the WPTS, intending to enhance the performance of the WPTS in the case of coil-couple malposition. The model of the transmission system is built and different coil arrangement methods are analyzed. Then, the magnetic field distributions of the proposed WPTS with different coil arrays are compared using numerical simulations. Experiments are conducted to investigate the performances of the designed WPTS. The results show that WPTS with a seven-coil array can provide a more uniform magnetic field for the WPTS, whose relative deviation of output power is less than 28.55%. This study provides some clues for improving the performance of the WPTS through different arrangements of the transmitter coils.

INDEX TERMS Wireless power transmission, magnetic field distribution, multi-transmitter coils array.

I. INTRODUCTION

Powering devices wirelessly has attracted increased attention for its high security and convenience, aiming to eliminate the wires and batteries limitations [1], [2]. WPTS has been applied in many fields, such as industrial robots [3], [4], [5], [6], [7], [8]. engineering applications, measurement science and technology [9], [10], [11], unmanned aerial vehicles [12], electric vehicles [13], [14], [15], medical devices [16], [17], etc. In the application of the automated guided vehicle, the position of the transmitter coil and receiver coil is commonly changed for the moving vehicle, affecting the performance of the WPTS. In the WPTS, electric power is transmitted based on the magnetic field produced by the transmitter coil. The uniformity of the magnetic flux density changes with the malposition of the coil-couple, leading to the variation of the received power [18], [19], [20]. How to enhance the performance against malposition is one of the most-researched subjects on the WPTS [21], as the malposition between the transmitter coil and receiver coil is inevitable in most WPTS [22].

Large-size transmitter coil is commonly designed to keep the receiver coil being strongly induced the malposition of the transmission coil-coupler in the WPTS [23], [24]. However, the magnetic flux density distribution is non-uniform, especially between the edge and center of the transmission area, leading to fluctuations in the received voltage at different positions. Feedback controls by adjusting the input power are employed in some WPTS to ensure stable received power, which is based on detecting the malposition of the transmission coil-coupler [25], [26], [27], [28], [29], [30]. However, sensors and controller are demanded [31], which undoubtedly increase the complexity of the system and tend to degrade the system efficiency. In addition, the magnetic field intensity in the transmission area can be stabilized by setting the arrangement of multiple transmitter

The associate editor coordinating the review of this manuscript and approving it for publication was Diego Masotti.

coils reasonably. In reference [32], an induction chain based on overlapping array was proposed to make 50% overlap between the transmitter coils to eliminate the weak point in the electromagnetic field during the movement of the receiving coil, and to ensure the uniformity of the magnetic field with high efficiency. Reference [33] proposed a self-tuning WPTS with multiple transmitter coils through the array of repeaters to provide the best power transmission for the mobile receiver. However, there are still limitations that the distance between the repeater array and the receiver must always be larger than the distance between the transmitter and the repeater, and the cross-coupling between the transmitter coils is ignored. Similarly, a novel double-layer honeycomb-like repeater coil array is proposed in reference [34], which can significantly improve the transmission efficiency compared with the single-layer honeycomb-like structure when the receiver position changes.

This paper presents a novel multi-transmitter coils array for WPTS, which requires no additional components to provide a more uniform magnetic field for the receiver coil, aiming to enhance the performance of the WPTS against the malposition of the transmission coil-couple. Comparing with the single transmitter coil, multi-coils are considered to provide more uniform magnetic field for its smaller edge effects. With the specific area for the transmitter coil, different position arrangements of the transmitter coils (with different numbers and diameters of transmitter coils), as well as the different electrical connections among the transmitter coils, are designed in this study. Numerical calculations of the proposed WPTS are carried out by COMSOL software, to obtain the magnetic field distributions. Accordingly, the magnetic flux density distributions are calculated and compared to determine the optimal coil arrangement. Experiments are conducted to investigate the performance of the proposed multi-transmitter coils by adjusting the position of the receiver coil. The results show that the transmitter coil array with seven coils has well comprehensive performance, whose relative deviation of output power is less than 28.55%. The remainder of this paper offers the following:

An analytical model of the WPTS is constructed to illustrate the energy transmission mechanism between the transmitter coils and receiver coil. In addition, different types of transmitter coil arrays are designed.

Numerical calculations and experiments are performed to analyze the performance of the proposed transmitter coil arrays. With the specific area of the transmitter coil, seven types of transmitter coils are tested. Then the magnetic field distributions and power transmission performances are provided.

II. OVERALL SYSTEM AND DESIGN TOPOLOGY DESCRIPTION

Figure 1 shows the topology of the proposed WPTS. It includes power supply, full-bridge inverter, transmitter resonance compensation, coil-couple, receiving resonance compensation, rectifier circuit, and load.

The transmitter side loop is composed of power supply, multiple transmitter (Tx) coils, full-bridge inverter, and compensation capacitance (C_T) of the Tx coils: the Tx coils are modeled by self-inductance (L_T), the full bridge inverter consists of MOSFETs ($VT_1 - VT_4$). The receiving side loop includes a receiving (Rx) coil, rectifier circuit, compensation capacitance (C_R) and load (R_L): the Rx coil is modeled by self-inductance (L_R), the rectifier circuit consists of diodes ($D_1 - D_4$). The full-bridge inverter eventually transforms the input direct current (DC) into the alternating current (AC) of the required frequency of the system by providing complimentary driving signals to the four MOSFETs, so that the transmitter side loop and the receiving side loop work in a resonant state, and then the receiving side loop receives the AC and converts it into the DC for the load through the rectifier and filter capacitance (C_f).

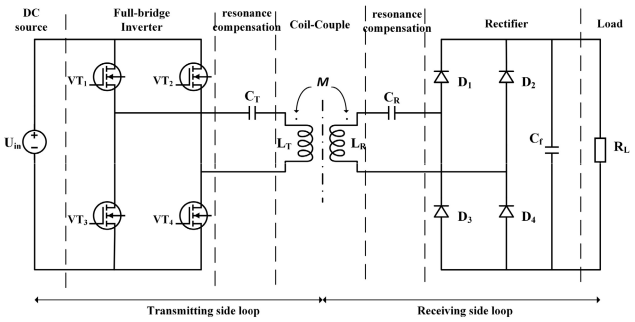

FIGURE 1. The topology of the proposed WPTS.

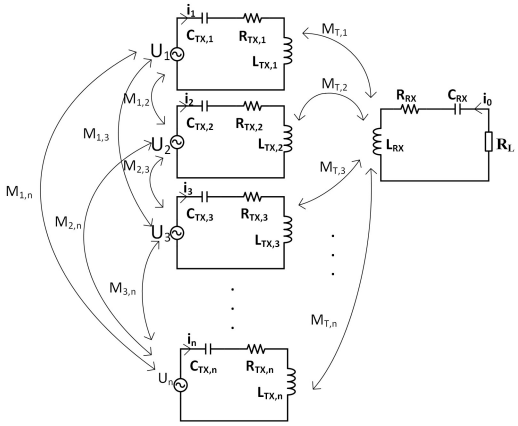

FIGURE 2. Equivalent circuit of the applied WPTS.

Figure 2 shows the simplified circuit of the WPTS with $n - T_x$ coils, where the transmitting side loop has the $n - \text{th}T_x$ coil with input voltage $U_n(n = 1, 2, 3\cdots)$, resonant capacitance $C_{TX,n}$, self-inductance of the transmitter coil $L_{TX,n}$, equivalent internal resistance $R_{TX,n}$, and $M_{m,n}(m, n = 1, 2, 3, \cdots)$ represents the mutual inductance between the $m - \text{th}T_x$ coil and the $n - \text{th}T_x$ coil. The receiving loop has a self-inductance of the receiving coil L_{RX}, equivalent internal resistance R_{RX}, resonant capacitance C_{RX}, load R_L,

and $M_{T,n}(n = 1, 2, 3, \cdots)$ represents the mutual inductance between the R_x coil and the $n-$thT_x coil.

Here, $M_{T,n} = k_{R,n}\sqrt{L_{TX,n}L_{RX}}$,and the $k_{R,n}$ is the coupling coefficient between the $n-$thT_x coil and the R_x coil.

When considering the condition of the cross-coupling between the Tx coils ($M_{m,n} \neq 0$). According to the Kirchhoff voltage law, the circuit equation can be achieved by as in (1), shown at the bottom of the page, [35], when the conditions of cross-coupling between Tx coils are ignored ($M_{m,n} = 0$). According to the Kirchhoff voltage law, the circuit equation can be achieved by as in (2), shown at the bottom of the page, where ω is the operating angular frequency, and $Z_{T,k}$ and Z_{RX} represent the reflected impedance of the transmitting and receiving circuits, respectively, the formula is as follows.

$$\begin{cases} Z_{T,k} = R_{TX,k} + j\omega L_{TX,k} + 1/j\omega C_{TX,k} \\ Z_{RX} = R_{RX} + j\omega L_{RX} + 1/j\omega C_{RX} + R_L \end{cases} \tag{3}$$

When the system is in resonance, the following formula can be obtained.

$$\begin{cases} j\omega L_{TX,1} + \frac{1}{j\omega C_{TX,1}} = 0 \\ j\omega L_{TX,2} + \frac{1}{j\omega C_{TX,2}} = 0 \\ \vdots \qquad\qquad \vdots \\ j\omega L_{TX,n} + \frac{1}{j\omega C_{TX,n}} = 0 \end{cases} \tag{4}$$

$$\begin{cases} i_1 = \frac{U_1 - j\omega M_{T,1} i_0}{R_{TX,1}} \\ i_2 = \frac{U_2 - j\omega M_{T,2} i_0}{R_{TX,2}} \\ \vdots \qquad\qquad \vdots \\ i_n = \frac{U_n - j\omega M_{T,n} i_0}{R_{TX,n}} \\ i_0 = \frac{j\omega M_{T,1} i_1 + j\omega M_{T,1} i_1 + \cdots + j\omega M_{T,n} i_n}{R_L + R_{RX}} = \frac{\sum_{k=1}^{n} j\omega M_{T,k} i_k}{R_L + R_{RX}} \end{cases} \tag{5}$$

Combining (2) - (5), the input power of the system P_{in}, the output power of the system P_{out} and the system transmission efficiency η can be calculated as (6).

$$\begin{cases} P_{in} = \sum_{k=1}^{n} U_k i_k \\ P_{out} = i_0^2 R_L = \left(\frac{\sum_{k=1}^{n} j\omega M_{T,k} i_k}{R_L + R_{RX}} \right)^2 R_L \\ \eta = \frac{P_{out}}{P_{in}} = \frac{R_L \left(\sum_{k=1}^{n} j\omega M_{T,k} i_k \right)^2}{(R_L + R_{RX})^2 \sum_{k=1}^{n} U_k i_k} \end{cases} \tag{6}$$

Theoretically, it follows from (6) that the output power and transmission efficiency of a multiple-transmitter coil magnetically coupled resonator depend on several factors, including the operating angular frequency, mutual inductance between the coils, the equivalent resistance of the transmitting and receiving sides, and the load. Thus, any change in these factors will result in a corresponding change in the transmission efficiency of a wireless power transfer system (WPTS). In actual automatic vehicle applications, it is difficult to precisely align the position of the receiving coil and the transmitter coil, leading to a decrease in their mutual inductance and consequently reducing the overall transmission efficiency of the system.

III. SYSTEM PARAMETER CHARACTERISTIC ANALYSIS

A. PLANAR SPIRAL COIL DESIGN

In this paper, the planar spiral coil is employed, as shown in Figure 3.

where D_{min} is the inner diameter of coil, D_{max} is the outer diameter of coil, D_{wire} is the diameter of conductor and D_{pitch} is the diameter of conductor.

According to the geometric parameters of the planar spiral coil in reference [36], the equivalent inductance of the coil

$$\begin{bmatrix} U_1 \\ U_2 \\ \vdots \\ U_n \\ 0 \end{bmatrix} = \begin{bmatrix} Z_{T,1} & j\omega M_{1,2} & \cdots & j\omega M_{1,n} & j\omega M_{T,1} \\ j\omega M_{1,2} & Z_{T,2} & \cdots & j\omega M_{2,n} & j\omega M_{T,2} \\ \vdots & \vdots & \ddots & \vdots & \vdots \\ j\omega M_{1,n} & j\omega M_{2,n} & \cdots & Z_{T,n} & j\omega M_{T,n} \\ j\omega M_{T,1} & j\omega M_{T,2} & \cdots & j\omega M_{T,n} & Z_{RX} \end{bmatrix} \times \begin{bmatrix} i_1 \\ i_2 \\ \vdots \\ i_n \\ i_0 \end{bmatrix} \tag{1}$$

$$\begin{bmatrix} U_1 \\ U_2 \\ \vdots \\ U_n \\ 0 \end{bmatrix} = \begin{bmatrix} Z_{T,1} & 0 & \cdots & 0 & j\omega M_{T,1} \\ 0 & Z_{T,2} & \cdots & 0 & j\omega M_{T,2} \\ \vdots & \vdots & \ddots & \vdots & \vdots \\ 0 & 0 & \cdots & Z_{T,n} & j\omega M_{T,n} \\ j\omega M_{T,1} & j\omega M_{T,2} & \cdots & j\omega M_{T,n} & Z_{RX} \end{bmatrix} \times \begin{bmatrix} i_1 \\ i_2 \\ \vdots \\ i_n \\ i_0 \end{bmatrix} \tag{2}$$

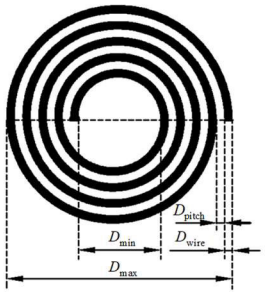

FIGURE 3. Geometric structure of planar spiral coil.

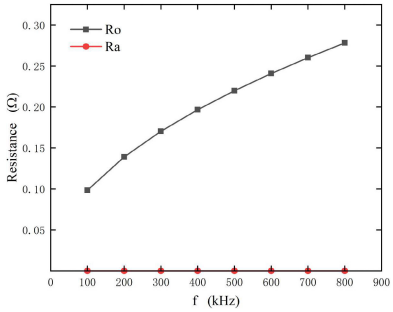

FIGURE 4. Relationship between frequency and ohmic resistance and radiation resistance.

can be obtained as follows.

$$\begin{cases} D_{avg} = \dfrac{D_{max} + D_{min}}{2} \\ \beta = \dfrac{D_{max} - D_{min}}{D_{max} + D_{min}} \\ L = \dfrac{\mu_0 N^2 D_{avg}}{2} \cdot \left(\ln \dfrac{2.46}{\beta} + 0.2\beta^2 \right) \end{cases} \tag{7}$$

where L is coil self-inductance, μ_0 is the magnetic permeability in vacuum, N is the turns of coil, β is the filling rate of wires, and D_{avg} is the average radius of coil.

The equivalent internal resistance R of the coil is composed of the ohmic resistance R_o and the radiation loss resistance R_a. R, R_o, and R_a can be expressed as follow the reference [36].

$$\begin{cases} R = R_O + R_a \\ R_o = \sqrt{\dfrac{\mu_0 \omega}{2\sigma}} \cdot \dfrac{N D_{avg}}{D_{wire}} \\ R_a = 340\pi^4 N^2 \cdot \left(\dfrac{\pi D_{avg}^2}{4\lambda^2} \right)^2 \end{cases} \tag{8}$$

where σ is the conductivity of the conductor and $\lambda = c/f$ is the wavelength corresponding to the operating frequency, and c is the speed of light.

As shown in (8), the equivalent internal resistance (R) of the system is related to the angular frequency (ω), wire diameter (D_{wire}), coil size, and number of turns (N). Taking the theoretical parameters of the Rx coil in Table 1 as an example, the relationship between frequency and ohmic resistance and radiation resistance is drawn, as shown in Figure 4, due to the coil of equivalent ohmic resistance (R_o) is much greater than the radiation loss resistance (R_a), therefore, the influence of radiation resistance can be ignored, $R = R_o$ can be obtained. Combining (3) and (4) reveals that near the resonant frequency, the inductive and capacitive components of the coil exhibit opposite trends in impedance. When the system is in resonance, the impedance of system is determined by the real part of the impedance. However, when the system deviates from the resonant frequency, the effective internal resistance changes primarily due to variations in the imaginary part of the impedance.

B. LAYOUT AND CONNECTION OF TRANSMITTER COILS

The arrangement of the transmitting pad proposed by us consists of 1 - 7 coils in series, in which the circular diameter formed by the arrangement of multiple coils is the same as that of the circular receiving coil. According to the research in references [37] and [38], the seven-coil array has the benefit of generating more uniform magnetic fields and lowering the degree of coupling between nearby transmitter coils. Therefore, we researched a circular array made up of seven coils, and Figure 5 depicts the actual coil arrangement.

The maximal outer ring approach is used to organize the transmitter coil. The maximum outer ring radius equals the maximum outer ring radius of the receiving coil. Table 1 shows the receiving coil's parameters. Under the assumption that the number of transmitter coil arrays is multiple, the number of turns, wire diameter, and turn spacing of each transmitter coil is kept uniform to compare the magnetic field distributions of different transmitter coil arrays. In a varied number of transmitter coil arrays, each coil has 15 turns with diameter of 1.5mm, the detailed parameters of each coil in different transmitter coil arrays are listed in Table 2. Where L_t is the theoretical inductance, L_s is the inductance in the simulation, R_t is the theoretical equivalent resistance, and R_s is the equivalent resistance in the simulation.

In order to eliminate the cross-coupling effect between multiple coils, mutual inductance and coupling coefficient are reduced by optimizing the coil spacing, as shown in Table 3. When the transmitter coil spacing is set to 10mm, the coupling coefficient between each coil in the transmitter coil array is effectively reduced with the given area between the transmitting and receiving sides. Therefore, the spacing between the coils is set to 10mm in our system.

IV. SIMULATION AND ANALYSIS

The proposed coil array's magnetic field distribution was analyzed using finite element in COMSOL Multiphysics simulation software under the position that $H = 5cm$, The simulation results are displayed in Figure 6.

As shown in Figure 6, a sphere with a radius of 300mm is set as the air domain in the finite element analysis software. The coil parameters are given in Table 2. In the array composed of seven different transmitter coils, the magnetic flux

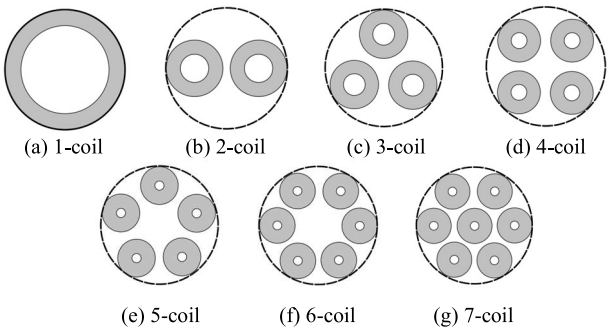

FIGURE 5. Layout diagram of transmitter coil array.

TABLE 1. Parameters of receiving coil.

Coil parameters	Theoretical value	Simulative value
N	15	15
$D_{wire}(mm)$	1.5	1.5
$D_{max}(cm)$	18	18
$D_{min}(cm)$	13.5	13.5
$L(\mu H)$	63.46	61.57
$R_{RX}(\Omega)$	0.26	0.24
Material	Copper	Copper

TABLE 2. Parameters of a single coil in the coil array.

coils	$D_{max}(cm)$	$D_{min}(cm)$	$L_t(\mu H)$	$L_s(\mu H)$	$R_t(\Omega)$	$R_s(\Omega)$
1	18	13.5	63.46	61.57	0.260	0.240
2	9	4.5	19.29	18.07	0.059	0.046
3	8	3.5	15.19	13.88	0.051	0.037
4	7	2.5	11.36	10.34	0.042	0.028
5	6.6	2.1	9.92	9.02	0.039	0.025
6	6	1.5	7.86	7.15	0.033	0.021
7	6	1.5	7.86	7.15	0.033	0.021

density is strongest in 1-coil, followed by 2-coil, and weakest in 6-coil. It can be found that the system with 7-coil provides a more uniform magnetic field.

To better illustrate the uniformity of the magnetic field, the relative deviation of the magnetic flux density, denoted as $E_B = (x, y, z)$, is introduced and described. The calculation formula is shown in (9), where $B(x, y, z)$ and $B(x_1, y_1, z_1)$ represent the magnetic flux density at a certain point in the air domain. When $B(x_1, y_1, z_1) = B(0, 0, 50)$, $E_B = (x, y, z_1)$ describes the degree of deviation of the magnetic flux density $B = (x, y, 50)$ from the magnetic flux density $B = (0, 0, 50)$ when the Rx coil is moving.

$$E_B(x, y, z_1) = \left| \frac{B(x_1, y_1, z_1) - B(x, y, z_1)}{B(x_1, y_1, z_1)} \right| \times 100\% \quad (9)$$

Simulations were conducted using COMSOL Multiphysics to calculate the relative deviations of points (70,0,50), (0,70,50), and (70,70,50) with respect to the center point (0,0,50) when the receiving coil is offset in the $x-y$ plane with a step size of 10mm. The results are shown in Table 4. The configuration

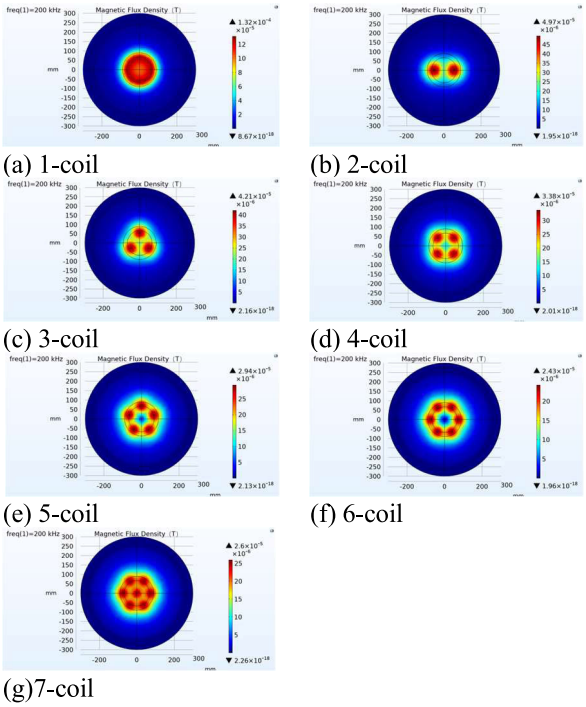

FIGURE 6. Magnetic field distribution with different arrangements of coils at $H = 5cm$.

TABLE 3. Coupling coefficient between coils at different spacing.

coils	Coil spacing (mm)	Mutual inductance (μH)	Coupling coefficient
2	0	0.7583	0.0409
	5	0.5824	0.0314
	10	0.4660	0.0251
3	0	0.5828	0.0400
	5	0.4373	0.0300
	10	0.3424	0.0235
4	0	0.4069	0.0375
	5	0.2953	0.0272
	10	0.2263	0.0208
5	0	0.3539	0.0374
	5	0.2529	0.0267
	10	0.1913	0.0202
6	0	0.2720	0.0363
	5	0.1892	0.0253
	10	0.1403	0.0188
7	0	0.2720	0.0363
	5	0.1892	0.0253
	10	0.1403	0.0188

with 7-coil exhibits the smallest relative deviation of the magnetic flux density, followed by 1-coil, while 6-coil shows the largest relative deviation. This indicates that the 7-coil provides better performance in case of the malposition between the transmitter coil and receiver coil.

From Figure 7, it can be observed that when the transmitter coil is directly aligned with the receiving coil, 1-coil exhibits the highest magnetic flux density, while 6-coil has the lowest. As the receiving coil deviates from the center of the array, 2-coil, 3-coil, 4-coil, 5-coil, and 6-coil show a

TABLE 4. Relative deviation of magnetic flux density.

Coil array	Magnetic flux density (μT)				Relative deviation		
	(0,0,50)	(70,0,50)	(0,70,50)	(70,70,50)	(70,0,50)	(0,70,50)	(70,70,50)
1	71.14	57.32	57.54	46.98	19.43%	19.11%	33.96%
2	24.23	42.10	12.96	18.23	73.76%	46.52%	24.76%
3	22.71	27.17	35.96	16.88	19.64%	58.33%	25.69%
4	13.34	18.56	18.95	24.21	39.21%	42.11%	81.56%
5	6.64	22.65	27.45	17.75	241.09%	313.36%	167.35%
6	2.62	23.07	16.61	18.91	780.92%	534.10%	621.87%
7	24.06	23.64	19.54	19.50	1.78%	18.80%	18.97%

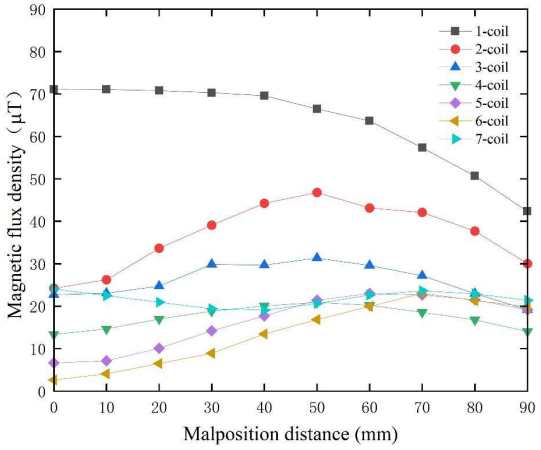

FIGURE 7. The magnetic flux intensity diagram.

TABLE 5. The mean and variance of the curve.

Number of transmitter coils	*mean* (μT)	*variance*
1	63.33	91.23
2	36.72	55.42
3	26.03	14.85
4	17.44	6.47
5	16.35	36.92
6	13.66	52.35
7	21.71	2.65

trend of increasing and then decreasing magnetic flux density, while 1-coil experiences a significant decrease, and 7-coil shows a trend of decreasing and then increasing. To better illustrate the fluctuations in the curves, Table 5 provides the mean value and variance of the magnetic field intensity under different transmission coil arrangements. The variance can be used to analyze the smoothness of the magnetic field intensity. During the malposition process, the mean value of the magnetic flux density shows a decreasing trend with an increasing number of transmitter coils (except for the 7-coil), and the 6-coil has the lowest average magnetic flux density. Furthermore, the 1-coil exhibits the highest variance, indicating significant fluctuations in the magnetic flux density, whereas the 4-coil and 7-coil have lower variances, indicating less fluctuation as the malposition distance increases. The arrangement with 7-coil exhibits the flattest magnetic field.

Based on the simulation results, it can be concluded that the uniformity of the magnetic field in a multi-transmitter coil array is also affected by the coil arrangement. Taking into account the stability of the magnetic field intensity when the R_x coil is offset from the T_x coil, the 7-coil configuration provides the lowest relative deviation of magnetic flux density and a more uniform magnetic field distribution, demonstrating better anti-malposition performance.

V. EXPERIMENTAL VALIDATION

A. EXPERIMENTS

To validate the simulation results, we constructed an experimental platform to investigate the performance of the proposed WPTS with different transmitter coils, as shown in Figure 8. The Electronic load (VICTOR-3801S) was utilized in the experiment to simulate the load. And the embedded microcontroller (STM32) was applied to drive the MOSFETs, as depicted in Figure 9. Finally, the performance of the proposed WPTS is analyzed by measuring the voltage and current changes of the receiving coil under different malposition distances. The main parameters of WPTS are shown in Table 4.

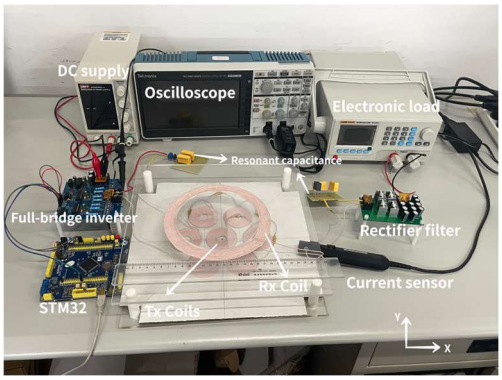

FIGURE 8. Experimental setup.

TABLE 6. Main parameter of WPTS.

Parameter	Note	Value
U_{in}	Input voltage	15V
f	Resonant frequency	200kHz
L_R	Inductance on the receiving side	62.29μH
C_R	Resonant capacitance on the receiving side	9.96nF
R_L	Load	10Ω

In the experiment, a full-bridge inverter was used to provide AC power to the WPTS, and the inverter voltage was observed by the oscilloscope (Tektronix-TBS2000), as shown in Figure 10. Besides, 400∗0.05mm litz wire was used to wind the coil. Figure 11 shows the arrangement and design of different coils, and the detailed physical parameters of transmitter coils are given in Table 7. Considering that the limitation of the transmitter coil area in the practical application, it was proposed to arrange multiple transmitter coils

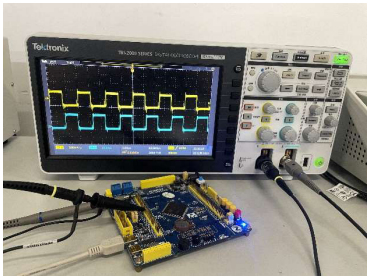

FIGURE 9. PWM drive signal generated by STM32.

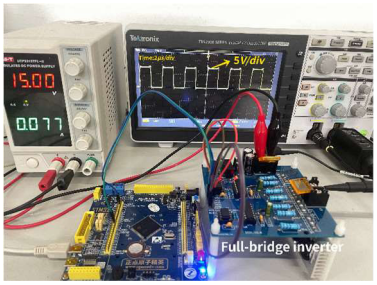

FIGURE 10. Full-bridge inverter voltage test.

under the same transmitting area, which was the maximum circumscribed circle method.

When the multi-transmitter coil array was aligned with the receiving coil, the voltage probe and current sensor (Tektronix-TCP2020) were used to collect the current and voltage signals of the transmitting loop and the receiving loop respectively. As shown in Figure 12, the voltage and current signals are in the same phase when the system resonates.

TABLE 7. Physical parameters of Coils.

Number of transmitter coils	*Inductance* (μH)	*Capacitance of compensation* (nF)	Equivalent resistance (Ω)
1	62.29	9.96	0.210
2	39.33	15.78	0.169
3	48.52	12.79	0.227
4	45.78	13.56	0.252
5	51.98	11.94	0.303
6	49.68	12.50	0.286
7	58.24	10.70	0.336
Receiving-coil	62.29	9.96	0.210

B. RESULT AND DISCUSSION

In recent years, the multi-coil array method has been proposed for the optimization of WPT systems misaligned at different positions. Table 8 provides a comprehensive comparison between the proposed method in this study and the previous research work.

The receiving coil was positioned in this experiment with a step size of 10mm and a 90mm horizontal offset along the positive axes of the X and Y axes (X and Y respectively represent the distance of horizontal deviation and the distance

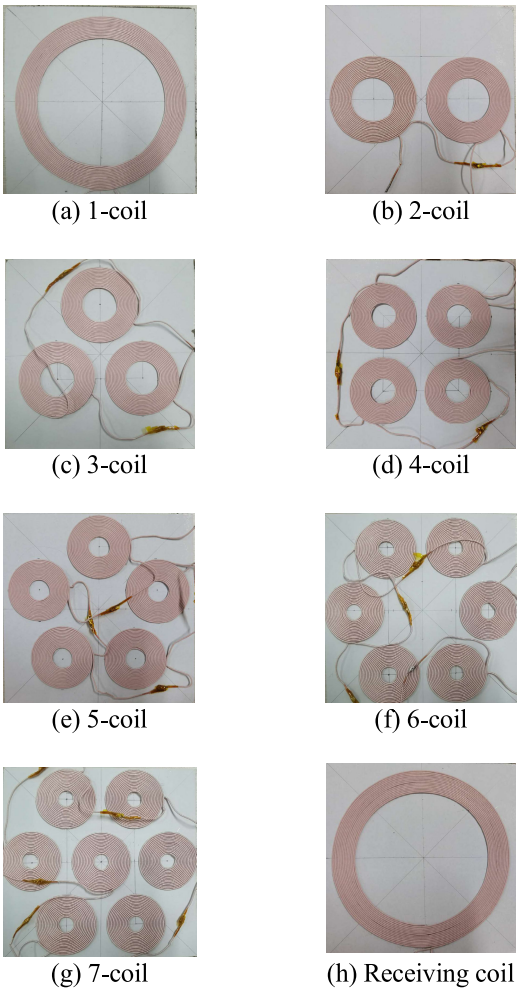

FIGURE 11. Layout diagram of transmitter coil array.

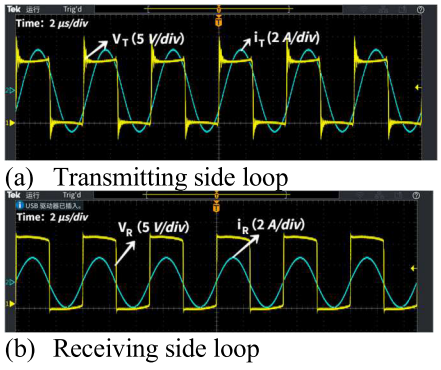

FIGURE 12. Experimental waveform.

of vertical deviation on the plane). The lateral offset distance of the receiving coil is shown in Figure 13. The relative output power deviation of the seven transmitter coils' output power curve is less than 28.55%, with a tiny range of fluctuation in the X-axis offset direction. The power transmitted by a single coil is the lowest, while the other transmitter coils all exhibit an upward trend. In the offset direction along the Y-axis,

except for the 2-coil, which exhibits a negative trend at the point of 70mm, the overall change in output power is roughly the same as that along the X-axis.

As a consequence, with the increase of malposition distance between coils, the output power of the multi-coil array also fluctuates, and the fluctuation of 4-coil and 2-coil is more obvious. whereas, the output power of the 7-coil changes little and fluctuates relatively steadily, which means that the 7-coil structure has better anti-malposition performance.

TABLE 8. Comparison with previous works.

Specific	This study	[39]	[40]	[32]	[33]	[41]
f（kHz）	200	64.25	125	900	14	13560
R_L（Ω）	10	4	20	82	2	5000
Layers of coils	Single	Double	Three	Double	Double	Three
Compensation network	S-S	S-S	LCC-S	S-S	S-S	P-P
Number of Tx coils	7	4	6	8	4	12
Malposition distance	X:90mm Y:90mm	X:120mm	Angle:150 degrees	Z:60mm	Y:180mm	X:25mm
H（mm）	50	50	20	40	80	70
P_{out}（W）	30	100	2.12	0.439	200	0.0054
Size of Rx area and Tx area	$S_{Rx} = S_{Tx}$	$S_{Rx} < S_{Tx}$	$S_{Rx} < S_{Tx}$	$S_{Rx} < S_{Tx}$	$S_{Rx} < S_{Tx}$	$S_{Rx} < S_{Tx}$
Application	Automated guided vehicle	High horizontal misalignment	Implantable medical drug pump	Free Moving Applications	Underwater vehicles	Implantable medical devices

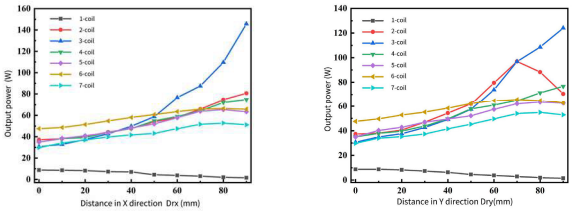

FIGURE 13. The relationship between malposition distance and output power.

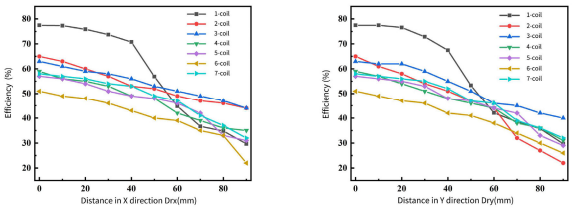

FIGURE 14. The relationship between malposition distance and transmission efficiency.

When the malposition distance is within 60mm, the single-transmitter coil provides the highest efficiency, as shown in Figure 14. However, when the malposition distance is 40mm, the efficiency of the single-transmitter coil rapidly declines. In contrast, there are only slight variations in the transmission efficiency of the seven-transmitter coils.

Combined with Figures 13 and 14, it can be found that single-coil and multi-coil have differences in transmission efficiency and output power. From the perspective of output power, multi-transmitter coils can transmit higher power than a single coil, and provides smoother power within a malposition distance of 60mm (except for the three-transmitter coil). In terms of transmission efficiency, a single-coil performs better than multi-transmitter coils up to a specific malposition distance, whereas multi-transmitter coils can extend the transmission distance of WPTS. Therefore, it can be found that multiple transmission coils can be used to reduce the sensitivity of WPTS to the malposition distance and increase the tolerance of the receiver position dislocation.

VI. CONCLUSION

In this paper, the magnetic field intensity of multiple transmitter coil arrays with different numbers is introduced. And the magnetic coupling resonator is modeled with the COMSOL Multiphysics software. Given the malposition of the coil in the process of wireless charging of the vehicle, the anti-malposition performance of the coil array is discussed through the analysis of the magnetic field distribution. Finally, the experimental prototype is constructed to verify the simulation results. The main research results are as follows:

1. The smoothness of the magnetic field intensity of the multiple transmitter coil arrays is not entirely dependent on the number of coils but also is affected by the arrangement of the coil array.

2. In the case of multi-transmitter coil arrays with a charging distance of 5cm, the experimental results show that the relative deviation of the output power of WPTS composed of seven transmitter coils is less than 28.55% within the malposition distance of 40mm. And the electromagnetic field simulation results show that the WPTS composed of seven-transmitter coils provide a more uniform flux density. Therefore, considering the uniformity of the magnetic field and the stability of the output power of WPTS, the seven-transmitter coils have the smallest flux density variation and the strongest ability to resist malposition.

In this study, the effects of different transmitter coil arrays on the transmission performance of WPTS are discussed, and the distributions of magnetic flux density are analyzed. It provides some clues for the exploration and research of wireless power transmission system with multi-coil structures.

REFERENCES

[1] A. M. Jawad, R. Nordin, and S. K. Gharghan, "Opportunities and challenges for near-field wireless power transfer: A review," *Energies*, vol. 10, no. 7, p. 1022, Jul. 2017, doi: 10.3390/en10071022.

[2] S. D. Barman, A. W. Reza, N. Kumar, M. E. Karim, and A. B. Munir, "Wireless powering by magnetic resonant coupling: Recent trends in wireless power transfer system and its applications," *Renew. Sustain. Energy Rev.*, vol. 51, pp. 1525–1552, Nov. 2015, doi: 10.1016/j.rser.2015.07.031.

[3] D. Kim, K. Hwang, J. Park, H. H. Park, and S. Ahn, "High-efficiency wireless power and force transfer for a micro-robot using a multiaxis AC/DC magnetic coil," *IEEE Trans. Magn.*, vol. 53, no. 6, pp. 1–4, Jun. 2017, doi: 10.1109/tmag.2017.2661992.

[4] H. Liu, X. Huang, L. Tan, J. Guo, W. Wang, C. Yan, and C. Xu, "Dynamic wireless charging for inspection robots based on decentralized energy pickup structure," *IEEE Trans. Ind. Informat.*, vol. 14, no. 4, pp. 1786–1797, Apr. 2018, doi: 10.1109/TII.2017.2781370.
[5] S.-J. Huang, T.-S. Lee, W.-H. Li, and R.-Y. Chen, "Modular on-road AGV wireless charging systems via interoperable power adjustment," *IEEE Trans. Ind. Electron.*, vol. 66, no. 8, pp. 5918–5928, Aug. 2019, doi: 10.1109/TIE.2018.2873165.
[6] M. T. Nguyen, C. V. Nguyen, and L. H. Truong, "Electromagnetic field based WPT technologies for UAVs: A comprehensive survey," *Electronics*, vol. 9, no. 3, p. 461, Mar. 2020, doi: 10.3390/electronics9030461.
[7] Y. Li, X. Ni, J. Liu, R. Wang, J. Ma, Y. Zhai, and Y. Huang, "Design and optimization of coupling coils for bidirectional wireless charging system of unmanned aerial vehicle," *Electronics*, vol. 9, no. 11, p. 14, Nov. 2020, doi: 10.3390/electronics9111964.
[8] M. Lu, M. Bagheri, A. P. James, and T. Phung, "Wireless charging techniques for UAVs: A review, reconceptualization, and extension," *IEEE Access*, vol. 6, pp. 29865–29884, 2018, doi: 10.1109/access.2018.2841376.
[9] Y. Wu, "Study on high frequency response characteristics of a moving-coil-type linear actuator using the coils combinations," *Hydromechatronics*, vol. 5, no. 3, pp. 226–242, 2022.
[10] P. F. Qian, H. Luo, L. Liu, P. Lv, and C. Pu, "A hybrid Gaussian mutation PSO with search space reduction and its application to intelligent selection of piston seal grooves for homemade pneumatic cylinders," *Eng. Appl. Artif. Intell.*, vol. 122, no. p. 14, Jun. 2023, doi: 10.1016/j.engappai.2023.106156.
[11] P. F. Qian, C. Pu, L. Liu, X. Li, and B. Zhang, "Development of a new high-precision friction test platform and experimental study of friction characteristics for pneumatic cylinders," *Meas. Sci. Technol.*, vol. 33, no. 6, p. 14, Jun. 2022, doi: 10.1088/1361-6501/ac51a6.
[12] H. Hussaini and C. Wang, "Battery energy storage system control and integration strategy for the more electric aircraft DC grid application," *Hydromechatronics*, vol. 5, no. 3, pp. 275–290, 2022.
[13] M. Rozman, A. Ikpehai, B. Adebisi, K. M. Rabie, H. Gacanin, H. Ji, and M. Fernando, "Smart wireless power transmission system for autonomous EV charging," *IEEE Access*, vol. 7, pp. 112240–112248, 2019, doi: 10.1109/access.2019.2912931.
[14] A. Mahesh, B. Chokkalingam, and L. Mihet-Popa, "Inductive wireless power transfer charging for electric vehicles—A review," *IEEE Access*, vol. 9, pp. 137667–137713, 2021, doi: 10.1109/access.2021.3116678.
[15] Z. Qiu, Y. Chen, X. Liu, L. Zhang, and H. Cheng, "Evaluation and comparison of sideband harmonics and acoustic responses with continuous and discontinuous PWM strategies in permanent magnet synchronous motor for electric vehicles," *Int. J. Hydromechatronics*, vol. 5, no. 2, pp. 109–123, 2022.
[16] R. V. Taalla, M. S. Arefin, A. Kaynak, and A. Z. Kouzani, "A review on miniaturized ultrasonic wireless power transfer to implantable medical devices," *IEEE Access*, vol. 7, pp. 2092–2106, 2019, doi: 10.1109/access.2018.2886780.
[17] S. R. Khan, S. K. Pavuluri, G. Cummins, and M. P. Y. Desmulliez, "Wireless power transfer techniques for implantable medical devices: A review," *Sensors*, vol. 20, no. 12, p. 58, Jun. 2020, doi: 10.3390/s20123487.
[18] Md. R. Basar, M. Y. Ahmad, J. Cho, and F. Ibrahim, "Stable and high-efficiency wireless power transfer system for robotic capsule using a modified Helmholtz coil," *IEEE Trans. Ind. Electron.*, vol. 64, no. 2, pp. 1113–1122, Feb. 2017, doi: 10.1109/TIE.2016.2614268.
[19] J. Zhou, B. Zhang, W. Xiao, D. Qiu, and Y. Chen, "Nonlinear parity-time-symmetric model for constant efficiency wireless power transfer: Application to a drone-in-flight wireless charging platform," *IEEE Trans. Ind. Electron.*, vol. 66, no. 5, pp. 4097–4107, May 2019, doi: 10.1109/TIE.2018.2864515.
[20] Q. Xu, Q. Hu, H. Wang, Z.-H. Mao, and M. Sun, "Optimal design of planar spiral coil for uniform magnetic field to wirelessly power position-free targets," *IEEE Trans. Magn.*, vol. 57, no. 2, pp. 1–9, Feb. 2021, doi: 10.1109/TMAG.2020.3042131.
[21] X. Lu, P. Wang, D. Niyato, D. I. Kim, and Z. Han, "Wireless charging technologies: Fundamentals, standards, and network applications," *IEEE Commun. Surveys Tuts.*, vol. 18, no. 2, pp. 1413–1452, 2nd Quart., 2016, doi: 10.1109/COMST.2015.2499783.
[22] C. Zheng, H. Ma, J.-S. Lai, and L. Zhang, "Design considerations to reduce gap variation and misalignment effects for the inductive power transfer system," *IEEE Trans. Power Electron.*, vol. 30, no. 11, pp. 6108–6119, Nov. 2015, doi: 10.1109/TPEL.2015.2424893.
[23] H. Hoang, S. Lee, Y. Kim, Y. Choi, and F. Bien, "An adaptive technique to improve wireless power transfer for consumer electronics," *IEEE Trans. Consum. Electron.*, vol. 58, no. 2, pp. 327–332, May 2012, doi: 10.1109/TCE.2012.6227430.
[24] D. Ahn, S.-M. Kim, S.-W. Kim, J.-I. Moon, and I.-K. Cho, "Wireless power transfer receiver with adjustable coil output voltage for multiple receivers application," *IEEE Trans. Ind. Electron.*, vol. 66, no. 5, pp. 4003–4012, May 2019, doi: 10.1109/TIE.2018.2833024.
[25] C. Liang, "Coil positioning for wireless power transfer system of automatic guided vehicle based on magnetic sensing," *Sensors*, vol. 20, no. 18, p. 5304, Sep. 2020, doi: 10.3390/s20185304.
[26] N. Khan, H. Matsumoto, and O. Trescases, "Wireless electric vehicle charger with electromagnetic coil-based position correction using impedance and resonant frequency detection," *IEEE Trans. Power Electron.*, vol. 35, no. 8, pp. 7873–7883, Aug. 2020, doi: 10.1109/TPEL.2020.2965476.
[27] L. Zhao, D. J. Thrimawithana, and U. K. Madawala, "Hybrid bidirectional wireless EV charging system tolerant to pad misalignment," *IEEE Trans. Ind. Electron.*, vol. 64, no. 9, pp. 7079–7086, Sep. 2017.
[28] Y. Chen, R. Mai, Y. Zhang, M. Li, and Z. He, "Improving misalignment tolerance for IPT system using a third-coil," *IEEE Trans. Power Electron.*, vol. 34, no. 4, pp. 3009–3013, Apr. 2019, doi: 10.1109/TPEL.2018.2867919.
[29] A. Azad, R. Tavakoli, U. Pratik, B. Varghese, C. Coopmans, and Z. Pantic, "A smart autonomous WPT system for electric wheelchair applications with free-positioning charging feature," *IEEE J. Emerg. Sel. Topics Power Electron.*, vol. 8, no. 4, pp. 3516–3532, Dec. 2020.
[30] Z. Yang, Y. Chen, D. Yang, W. Du, G. He, X. Zhang, C. Xu, and W. Wang, "Research on parameter optimization of double-D coils for electric vehicle wireless charging based on magnetic circuit analysis," *IEICE Electron. Exp.*, vol. 17, no. 7, 2020, Art. no. 20200067, doi: 10.1587/elex.17.20200067.
[31] P. Qian, C. Pu, L. Liu, P. Lv, and L. M. R. Páez, "A novel pneumatic actuator based on high-frequency longitudinal vibration friction reduction," *Sens. Actuators A, Phys.*, vol. 344, Sep. 2022, Art. no. 113731, doi: 10.1016/j.sna.2022.113731.
[32] S. Pahlavan, M. Shooshtari, M. Maleki, and S. J. Ashtiani, "Using overlapped resonators in wireless power transfer for uniform electromagnetic field and removing blank spots in free moving applications," *Electronics*, vol. 11, no. 8, p. 1204, 2022, doi: 10.3390/electronics11081204.
[33] X. Dang, P. Jayathurathnage, S. A. Tretyakov, and C. R. Simovski, "Self-tuning multi-transmitter wireless power transfer to freely positioned receivers," *IEEE Access*, vol. 8, pp. 119940–119950, 2020, doi: 10.1109/access.2020.3005657.
[34] W. Xin, C. C. Mi, F. He, M. Jiang, and D. Hua, "Investigation of negative permeability metamaterials for wireless power transfer," *AIP Adv.*, vol. 7, no. 11, p. 2017, Nov. 2017, doi: 10.1063/1.5010218.
[35] S.-J. Jeon and D.-W. Seo, "Effect of additional transmitting coils on transfer distance in multiple-transmitter wireless power transfer system," *IEEE Access*, vol. 10, pp. 9174–9183, 2022, doi: 10.1109/access.2022.3144179.
[36] L. L. Tan, "Optimization design for disc resonators of a wireless power transmission system," *Trans. China Electrotechnical Soc.*, vol. 28, no. 8, p. 7, 2013.
[37] Q. Xu, Z. Gao, H. Wang, J. He, Z.-H. Mao, and M. Sun, "Batteries not included: A mat-based wireless power transfer system for implantable medical devices as a moving target," *IEEE Microw. Mag.*, vol. 14, no. 2, pp. 63–72, Mar. 2013.
[38] N. Sato, H. Kifune, and S. Komeda, "A coil layout of wireless power transfer systems based on multicoil arrangement for underwater vehicles," *Electr. Eng. Jpn.*, vol. 207, no. 2, pp. 38–48, Apr. 2019, doi: 10.1002/eej.23205.
[39] C. Sritongon, P. Wisestherrakul, N. Hansupho, S. Nutwong, A. Sangswang, S. Naetiladdanon, and E. Mujjalinvimut, "Novel IPT multi-transmitter coils with increase misalignment tolerance and system efficiency," in *Proc. IEEE Int. Symp. Circuits Syst. (ISCAS)*, May 2018, pp. 1–5, doi: 10.1109/ISCAS.2018.8351305.
[40] J. Rhee, Y. Shin, S. Woo, C. Lee, D. Kim, J. Ahn, H. Kim, and S. Ahn, "Wireless torque and power transfer using multiple coils with LCC-S topology for implantable medical drug pump," *Sensors*, vol. 21, no. 23, p. 8150, Dec. 2021, doi: 10.3390/s21238150.
[41] B. Lee, D. Ahn, and M. Ghovanloo, "Three-phase time-multiplexed planar power transmission to distributed implants," *IEEE J. Emerg. Sel. Topics Power Electron.*, vol. 4, no. 1, pp. 263–272, Mar. 2016, doi: 10.1109/JESTPE.2015.2436391.

QI LE was born in Jiangxi, China, in 1997. He received the B.S. degree in mechanical and automotive engineering from the Zhejiang University of Water Resources and Electric Power, Hangzhou, China, in 2021. He is currently pursuing the master's degree with the Zhejiang University of Science and Technology, Hangzhou. His research interests include wireless power transfer technology and power electronics converters.

RUIMING WU was born in Zhejiang, China, in 1970. He received the Ph.D. degree in mechanical engineering from Zhejiang University, Hangzhou, China, in 2005. He is currently an Associate Professor with the School of Mechanical and Energy Engineering, Zhejiang University of Science and Technology, Hangzhou. His research interest includes intelligent equipment manufacturing.

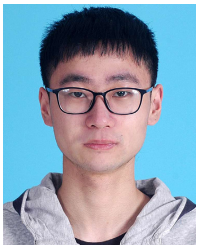

JIANGYU CHEN was born in Zhejiang, China, in 1999. He received the B.S. degree in mechanical and energy engineering from the Zhejiang University of Science and Technology, Hangzhou, China, in 2021, where he is currently pursuing the master's degree. His research interest includes wireless power transfer technology.

MEILING HUANG was born in Fujian, China, in 1997. She received the B.S. degree in electronic information engineering from Shandong Technology and Business University, Shandong, China, in 2019, and the M.S. degree in mechanical and energy engineering from the Zhejiang University of Science and Technology, Hangzhou, China, in 2021. Her research interests include wireless power transfer technology and nonlinear analysis.

YANG FU was born in Zhejiang, China, in 1987. He received the Ph.D. degree in mechanical electronic engineering from Zhejiang University, Hangzhou, China, in 2015. He is currently an Associate Professor with the School of Mechanical and Energy Engineering, Zhejiang University of Science and Technology, Hangzhou. His research interests include electromechanical system control and intelligent manufacturing.

FENG HUANG was born in Zhejiang, China, in 1986. He received the Ph.D. degree in mechanical electronic engineering from Zhejiang University, Hangzhou, China, in 2014. He is currently an Associate Professor with the School of Mechanical and Energy Engineering, Zhejiang University of Science and Technology, Hangzhou. His research interest includes intelligent manufacturing.

LIJUN WANG was born in Zhejiang, China, in 1984. He received the Ph.D. degree in mechanical electronic engineering from Zhejiang University, Hangzhou, China, in 2013. He is currently a Lecturer with the School of Automation and Electrical Engineering, Zhejiang University of Science and Technology, Hangzhou. His research interest includes electrical automation.

SHAN DU was born in Zhejiang, China, in 1988. She received the M.S. degree in project management from Zhejiang Gongshang University, Hangzhou, China, in 2018. She is currently the Director of Zhejiang Linix Motor Company Ltd.

QIPENG LI was born in Shandong, China, in 1977. He received the Ph.D. degree in mechanical electronic engineering from Zhejiang University, Hangzhou, China, in 2005. He is currently a Professor with the School of Mechanical and Energy Engineering, Zhejiang University of Science and Technology, Hangzhou. His research interest includes intelligent equipment manufacturing.